Free Radical Biology and Medicine 181 (2022) 197–208

Contents lists available at ScienceDirect

Free Radical Biology and Medicine

journal homepage: www.elsevier.com/locate/freeradbiomed

T3-induced enhancement of mitochondrial Ca^{2+} uptake as a boost for mitochondrial metabolism

Ines Tawfik [a,1], Benjamin Gottschalk [a,1], Angelo Jarc [a], Doruntina Bresilla [a], Rene Rost [a], Barbara Obermayer-Pietsch [b], Wolfgang F. Graier [a,c], Corina T. Madreiter-Sokolowski [a,*]

[a] Molecular Biology and Biochemistry, Gottfried Schatz Research Center, Medical University of Graz, Neue Stiftingtalstraße 6, 8010, Graz, Austria
[b] Department of Internal Medicine, Division of Endocrinology and Diabetology, Endocrinology Lab Platform, Medical University of Graz, Auenbruggerplatz 15, 8010, Graz, Austria
[c] BioTechMed, Graz, Austria

ARTICLE INFO

Keywords:
Mitochondrial Ca^{2+} homeostasis
Triiodothyronine
Uncoupling protein 2
Energy metabolism
ROS production

ABSTRACT

Thyroid hormones act as master regulators of cellular metabolism. Thereby, the biologically active triiodothyronine (T3) induces the expression of genes to enhance mitochondrial metabolic function. Notably, Ca^{2+} ions are necessary for the activity of dehydrogenases of the tricarboxylic acid cycle and, thus, mitochondrial respiration.

We investigated whether treating HeLa cells with T3 causes alterations in mitochondrial Ca^{2+} ($[Ca^{2+}]_{mito}$) levels. Real-time measurements by fluorescence microscopy revealed that treatment with T3 for 3 h induces a significant increase in basal $[Ca^{2+}]_{mito}$ levels and $[Ca^{2+}]_{mito}$ uptake upon the depletion of the endoplasmic reticulum (ER) Ca^{2+} store, while cytosolic Ca^{2+} levels remained unchanged. T3 incubation was found to upregulate mRNA expression levels of uncoupling proteins 2 and 3 (UCP2, UCP3) and of protein arginine methyltransferase 1 (PRMT1). Live-cell imaging revealed that T3-induced enhancement of mitochondrial Ca^{2+} uptake depends on the mitochondrial Ca^{2+} uniporter (MCU), UCP2, and PRMT1 that are essential for increased mitochondrial ATP ($[ATP]_{mito}$) production after T3 treatment. Besides, increased $[Ca^{2+}]_{mito}$ and $[ATP]_{mito}$ levels correlated with enhanced production of reactive oxygen species (ROS) in mitochondria. Notably, ROS scavenging causes mitochondrial Ca^{2+} elevation and outplays the impact of T3 on $[Ca^{2+}]_{mito}$ homeostasis.

Based on these results, we assume that thyroid hormones adjust $[Ca^{2+}]_{mito}$ homeostasis by modulating the UCP2- and PRMT1-balanced $[Ca^{2+}]_{mito}$ uptake via MCU in case of physiological ROS levels to convey their impact on mitochondrial ATP and ROS production.

1. Introduction

Thyroid hormones (TH) are crucial for organ development and metabolic control. Thereby, the biologically active 3,5,3'-triiodothyronine (T3) displays its pleiotropic effects on various cell types throughout the whole body [1]. T3 binds to thyroid hormone receptors (TRs) α or β, which then dock to thyroid hormone response elements within the regulatory regions of respective genes to modulate gene transcription [1]. Besides these so-called canonical effects, T3 also affects intracellular signaling pathways without DNA binding and subsequent induction of gene and protein expression [2].

T3 has been shown to promote the expression and nuclear translocation of the intermediate factors like nuclear respiratory factors (NRF) 1 [3] and the NRF2 [4], facilitating the maintenance and transcription of mitochondrial DNA (mtDNA). Moreover, T3 enhances the phosphorylation and nuclear translocation of NRF2. Besides, T3 mediates the expression of the transcriptional coactivator peroxisome proliferator-activated receptor-gamma coactivator-1 α (PGC-1α) [5], which is central for mitochondrial homeostasis by promoting nuclear- and mtDNA-encoded genes and buffering oxidative stress [6]. Moreover, a ubiquitously expressed mitochondrial matrix-located T3 receptor, p43, stimulates mitochondrial transcription and protein synthesis in the presence of T3 [7]. Based on these transcriptional modulations, thyroid hormones essential control mitochondrial function. In general, thyroid hormones facilitate the mitochondrial substrate oxidation and the catabolism of carbohydrates and lipids [8], promoting the tricarboxylic acid (TCA) cycle flux [9] and stimulating mitochondrial respiration and

* Corresponding author.
E-mail address: corina.madreiter@medunigraz.at (C.T. Madreiter-Sokolowski).
[1] Equally contributed.

https://doi.org/10.1016/j.freeradbiomed.2022.01.024
Received 30 November 2021; Received in revised form 13 January 2022; Accepted 24 January 2022
Available online 26 January 2022

Abbreviations

ATP	adenosine triphosphate
DMEM	Dulbecco's Modified Eagle Medium
ETC	electron transport chain
FCCP	carbonyl cyanide-p-trifluoromethoxyphenylhydrazone
fT3	free T3
Fura-2AM	Fura-2 acetoxy-methyl-ester
IBM	inner boundary membrane
IP3	inositol 1,4,5-triphosphate
LETM1	leucine zipper-EF-hand-containing transmembrane protein 1
MCU	mitochondrial Ca^{2+} uniporter
mtDNA	mitochondrial DNA
OCR	oxygen consumption rate
OXPHOS	oxidative phosphorylation
PRMT1	protein methyltransferase 1
ROI	region of interest
ROS	reactive oxygen species
T3	3,5,3'-triiodothyronine
TCA	tricarboxylic acid
TH	thyroid hormone
TMRM	tetramethylrhodamine
TR	thyroid hormone receptor
UCP1	uncoupling protein 1
UCP2	uncoupling protein 2
UCP3	uncoupling protein 3

oxidative phosphorylation (OXPHOS) [10]. Due to the leakage of protons from the intermembrane space into the matrix, so-called uncoupling, enhanced mitochondrial respiration is not strictly translated into adenosine triphosphate (ATP) production [11]. The basal proton-leak rate is regulated by the fatty-acyl composition of the inner mitochondrial membrane (IMM). At the same time, activation of specific proteins modulates the inducible proton-leak [8]. For example, the uncoupling protein 1 (UCP1), also known as thermogenin, allows proton-flux from the intermembrane space into the matrix of brown adipocytes. Thereby energy can't be used for ATP production via the ATP synthase but gets converted into heat instead [12]. Notably, several promoter regions of the Ucp1 gene exhibit thyroid hormone response elements [13], allowing thyroid hormones to stimulate the expression of the Ucp1 gene by transcriptional and post-transcriptional mechanisms. Consequently, thyroid hormones are necessary for cold-induced adaptive thermogenesis [14]. While the role of UCP1 in adipocytes is well-characterized, the function of its orthologues, uncoupling protein 2 (UCP2) and uncoupling protein 3 (UCP3), is still under debate. In contrast to UCP1, UCP2 is ubiquitously expressed, and UCP3 is predominantly found in skeletal muscle [15]. While UCP1 accounts for up to 10% of the IMM proteins in adipocytes, the amounts of UCP2 and UCP3 account for merely 0.01%–0.1% in the respective cell types [16]. Consequently, efficient uncoupling seems hardly possible, and several groups failed to detect uncoupling activity [17,18]. While the function of the distinct isoforms might be different, the expression of UCP2 and UCP3 seems to be controlled by thyroid hormones, similar to UCP1 [19]. Treatment of young, healthy males with T3 for 14 days induced UCP2 and UCP3 mRNA expression in skeletal muscle and adipose tissues [20]. Besides, administration of T3 to hypothyroid and euthyroid mice for six days enhanced UCP2 and UCP3 mRNA expression in the liver, skeletal muscle, and the heart. Notably, the level of UCP2 and UCP3 directly correlated with the resting metabolic rate [21]. Also, treatment of rats with T3 for 14 days resulted in enhanced UCP2 and UCP3 mRNA and protein expression levels as well as in enhanced mitochondrial ATP production in oxidative muscles [22]. In contrast, patients with hypothyroidism exhibited reduced UCP2 mRNA expression levels in comparison to people with a euthyroid state, and a correlation between lipid oxidation rates and UCP2 expression was revealed [23]. These studies demonstrate that T3 controls UCP2 and UCP3 expression and oppose the hypothesis that UCP2 and UCP3 function as uncouplers.

Reports have suggested that UCP2 and UCP3 might act as transporters for fatty acids [24,25] or TCA cycle intermediates [26], thereby modulating mitochondrial metabolic activity. Besides, UCP2 and UCP3 have been shown to enable proper mitochondrial Ca^{2+} ($[Ca^{2+}]_{mito}$) uptake in cells with hampered $[Ca^{2+}]_{mito}$ uptake due to protein methyltransferase 1 (PRMT1)-driven methylation of the Ca^{2+}-sensing mitochondrial Ca^{2+} uptake 1 (MICU1) [27]. Thereby, UCP2 and UCP3 facilitate $[Ca^{2+}]_{mito}$ uptake via the central pore-forming mitochondrial Ca^{2+} uniporter (MCU) [28]. Besides, alternative $[Ca^{2+}]_{mito}$ uptake routes involve the leucine zipper-EF-hand-containing transmembrane protein 1 (LETM1) [29]. This complex interaction allows to tightly control $[Ca^{2+}]_{mito}$ that acts as a powerful buffer for cytosolic Ca^{2+} and as a modulator of mitochondrial membrane potential [30], apoptotic signaling [31], and mitochondrial metabolic activity [32]. $[Ca^{2+}]_{mito}$ is essential to the function of Ca^{2+}-dependent dehydrogenases like pyruvate dehydrogenase [33], isocitrate dehydrogenase [34], and α-ketoglutarate dehydrogenase [35] of the TCA-cycle, facilitating the activity of the electron transport chain (ETC) by providing reduction equivalents [32]. Thereby, $[Ca^{2+}]_{mito}$ also affects the primary source of cellular production of reactive oxygen species (ROS). However, enhanced ETC activity does not *per se* translate into a higher probability of electron leakage and ROS production but is dependent on substrate and O_2 availability, mitochondrial membrane potential, and the functionality of the ETC [36]. Under physiological conditions, experiments revealed that Ca^{2+} diminishes ROS leakage from complex I and complex III. However, $[Ca^{2+}]_{mito}$ enhances ROS production in case of a blockage of ETC complexes [37]. In turn, ROS were also found to affect $[Ca^{2+}]_{mito}$ homeostasis by, for instance, oxidation of MCU leading to enhanced mitochondrial Ca^{2+} uptake [38].

In this study, we analyzed how T3 treatment affects $[Ca^{2+}]_{mito}$ homeostasis. This work reveals that T3-induced upregulation of UCP2, UCP3, and PRMT1 correlates with elevated basal $[Ca^{2+}]_{mito}$ levels and increased $[Ca^{2+}]_{mito}$ uptake. Moreover, we present that an increase in mitochondrial ATP ($[ATP]_{mito}$) production by T3 is dependent on proper $[Ca^{2+}]_{mito}$ uptake facilitated by UCP2, MCU, and PRMT1.

2. Material and methods

2.1. Cell culture and handling

HeLa cells and HeLa UCP2ko cells [39] were cultured in Dulbecco's Modified Eagle Medium (DMEM, D5523) (Sigma-Aldrich, Vienna, Austria), containing 10% fetal bovine serum (FCS) (Gibo, Lifetechnologies, Vienna, Austria), 4 mM glutamine, 5.5 mM glucose, 1% penicillin (100 U/ml) (Gibco), 1% streptomycin (100 μg/ml) (Gibco), and 1.25 μg/ml amphotericin B (Gibco). Cells were transiently transfected at a confluence of 60 to 70% with 1.5 μg plasmid DNA and 100 μM of respective siRNA using 2.5 μl of TransFast™ transfection reagent (Promega, Mannheim, Germany) in 1 ml of serum- and antibiotic-free DMEM. siRNAs were obtained from Microsynth (Balgach, Switzerland) and included human MCU siRNA-1: 5′-GCC AGA GAC AGA CAA UAC U dTdT-3′; human MCU siRNA-2: 5′-GGA AAG GGA GCU UAU UGA A dTdT-3′, human PRMT1 siRNA: 5′-CGU CAA AGC CAA CAA GUU A dTdT-3′, human UCP2 siRNA: 5′- GCA CCG UCA AUG CCU ACA A dTdT-3′ and human control siRNA: 5′- UUC UCC GAA CGU GUC ACG U dTdT-3′. Knockdown efficacy was validated previously [27]. 3,5,

3'-triiodothyronine (T3) was obtained from Sigma Aldrich (Missouri, US) and dissolved in ethanol and 1 M HCl (4:1). Cells were treated with 100 nM T3 in a culture medium containing FCS for different duration periods, including 3 h, 24 h, and 48 h. Control HeLa cells were treated with the respective T3-free stock solution. The treatment with 5 mM N-acetyl cysteine (NAC) was performed in parallel to the T3 treatment in a culture medium containing FCS.

2.2. Live-cell imaging experiments

For live-cell imaging experiments, cells were seeded on 30 mm glass coverslips in 6-well plates and accordingly transfected with 1.5 μg of plasmid DNA and 100 μM of the respective siRNA. Before the measurement, cells were kept in EH-loading buffer (135 mM NaCl, 5 mM KCl, 2 mM $CaCl_2$, 1 mM $MgCl_2$, 10 mM HEPES, 2.6 mM $NaHCO_3$, 440 μM KH_2PO_4, 340 μM Na_2HPO_4, 10 mM D-glucose, 0.1% MEM vitamins (Gibco), 0.2% MEM amino acids (Gibco), 1% penicillin-streptomycin (100 U/ml), 1% streptomycin (100 μg/ml), and 1.25 μg/ml amphotericin B, pH adjusted to 7.4) at room temperature. During the measurement, the cells were continuously perfused with a Ca^{2+}-containing buffer, which consisted of 145 mM NaCl, 5 mM KCl, 2 mM $CaCl_2$, 1 mM $MgCl_2$, 10 mM D-glucose, and 10 mM HEPES, pH adjusted to 7.4, using a perfusion system (PS9D, NGFI, Graz, Austria; www.ngfi.eu).

2.3. Measurements of $[Ca^{2+}]_{mito}$, $[ATP]_{mito}$, and mitochondrial membrane potential

Dynamic changes in $[Ca^{2+}]_{mito}$ were analyzed in Hela cells expressing the organelle-targeted FRET-based Ca^{2+} sensor 4mtD3cpv as previously described [27]. Cells were stimulated with the IP3-generating agonist ATP (Sigma Aldrich, Vienna, Austria). Basal levels in $[ATP]_{mito}$ were measured in Hela cells expressing the organelle-targeted FRET-based ATP sensor mtAT1.03 [40]. To determine mitochondrial membrane potential, cells were incubated in 20 nM of the fluorescent indicator tetramethylrhodamine (TMRM) (Invitrogen™ T668; Vienna, Austria) in EH-loading buffer for 20 min at room temperature, as described previously [41]. A full disruption of the mitochondrial membrane potential by application of carbonyl cyanide-p-trifluoromethoxyphenylhydrazone (FCCP) (Abcam, Cambridge, UK) was used to normalize the $TMRM_{mito}/TMRM_{nuc}$ ratio.

Measurements were performed on an inverted wide-field microscope (Observer.A1, Carl Zeiss GmbH, Vienna, Austria) as described previously [27,40,41]. Alternatively, an NGFI AnglerFish C-Y7G imager equipped with the NGFI PS9D perfusion system (NGFI) was used. In short, cells were imaged with a 40x oil immersion objective (Plan Apochromat 1,3 NA Oil DIC (UV) VISIR, Carl Zeiss GmbH, Vienna, Austria) and a standard CFP/YFP filter cube. Emission was collected with a 505dcxr beam-splitter on two sides of the camera (CCD camera, Coolsnap Dyno, Photometrics, Tucson, AZ, USA). 4mtD3cpv and mtAT1.03 were excited with a wavelength of 440 nm (440AF21, Omega Optical, Brattleboro, VT, USA), and emission was captured at 480 and 535 nm (480AF30 and 535AF26, Omega Optical, Brattleboro, VT, USA). TMRM was excited at 550 nm, and the emission was collected at 600 nm. A region of interest containing the mitochondrial TMRM fluorescence ($TMRM_{mito}$) and the cytosolic TMRM (generally the area of the nucleolus) fluorescence ($TMRM_{nuc}$) was selected, and a ratio $TMRM_{mito}/TMRM_{nuc}$ was calculated over time.

The data were recorded with the NIS-Elements AR software (Nikon, Vienna, Austria) and analyzed using GraphPad Prism (GraphPad Software, San Diego, CA). Measurements were background corrected using a background region of interest and corrected for bleaching using an exponential decay fit of the basal fluorescence extrapolated to the whole measurement. Results are shown as $\Delta max(TMRM_{mito}/TMRM_{nuc})$ between basal level and maximal FCCP induced depolarization.

Measurements of $[Ca^{2+}]_{cyto}$ and $[H_2O_2]_{mito}$

To measure $[Ca^{2+}]_{cyto}$, cells were incubated with the fluorescent cytosolic Ca^{2+} indicator Fura-2 acetoxy-methyl-ester (Fura-2AM) (TEFLabs, Austin, TX) for 30 min in EH-loading buffer, as described previously [42]. Fura-2AM was illuminated with 340 nm and 380 nm, and emission was captured at 515 nm (495dcxru; Omega Optical, Brattleboro, VT, USA). The results of the measurements were recorded with live-acquisition software v2.0.0.12 (Till Photonics) and analyzed using GraphPad Prism (GraphPad Software 9.3.0, San Diego, CA). The measurement was background-subtracted using a background ROI and corrected for bleaching using an exponential decay fit. Results are shown as the ratio of F_{380}/F_{340}.

Cells expressing the mitochondrial H_2O_2 sensor HyPer [43] were illuminated at 430 and 480 nm, whereas fluorescence emission was recorded at 520 nm. In order to normalize to maximal mitochondrial ROS levels, 150 μM of H_2O_2 were applied at the end of each measurement. The results of the measurements were recorded with live-acquisition software v2.0.0.12 (Till Photonics) and analyzed using GraphPad Prism (GraphPad Software 9.3.0, San Diego, CA). The measurement was background-subtracted using a background ROI and corrected for bleaching using an exponential decay fit. Results of ROS measurements are shown as the ratio of F_{480}/F_{430}.

Measurements in Fura-2AM stained cells and cells expressing mitochondrial HyPer were performed on a polychromator illumination system (VisiChrome, Visitron Systems, Puchheim, Germany) with a motorized sample table of Till Photonics (Graefling, Germany). Alternatively, an NGFI AnglerFish F/O imager (NGFI) equipped with the NGFI PS9D perfusion system was used. The probes were excited via a polychrome V (Till Photonics), and emission was visualized using a 40x objective (alpha Plan Fluar 40, Zeiss, Goettingen, Germany) and a charge-coupled device camera (AVT Stringray F145B, Allied Vision Technologies, Stadtroda, Germany).

2.4. Analyses of mitochondrial structure and ER-mitochondrial colocalization

Cells expressing ERAT4.03 NA (NGFI, Graz, Austria) were stained with 100 nM TMRM in EH-loading buffer for 20 min and 3D-imaged on a confocal spinning microscope (Axio Observer.Z1 from Zeiss, Gottingen, Germany) with z increments of 0.2 μm as previously described [39,44]. The microscope is equipped with a motorized filter wheel (CSUX1FW, Yokogawa Electric Corporation, Tokyo, Japan) on the emission side and a 100x objective lens (Planapochromat 100x/1.4 Oil, Zeiss, Germany). It also contains an AOTF-based laser merge module for laser lines 405, 445, 473, 488, 514, and 561 nm (Visitron Systems, Puchheim, Germany) and a Nipkow-based confocal scanning unit (CSU-X1, Yokogawa Electric Corporation). All images were taken with a CoolSnap HQ2-CCD camera (Photometrics, Tucson, Arizona, USA). Data acquisition and software control was achieved by VisiView Premier Acquisition software (2.0.8, Visitron Systems, Puchheim, Germany). Image stacks were deconvoluted through blind deconvolution (NIS-Elements 5.20.02, Nikon, Austria). Morphology parameters were measured automatically via a custom-made ImageJ macro using the following procedure. An additional background subtraction based on the rolling ball method was introduced to enhance contrast for later analysis. A global auto Otsu threshold using a stack histogram as well as a local auto Otsu threshold (radius of 640 nm) based on a single slice histogram were applied to the stack and merged. ERAT4.03 NA staining was Otsu thresholded, dilated, filled, and subsequently and used as a mask for TMRM stained mitochondria to exclude not transfected cells.

Binarized mitochondria got segmented via the ImageJ plugin 3D manager. Mitochondrial volume and surface were determined through the plugin 3D Geometrical Measure. The Plugin 3D Ellipsoid Fitting generated an ellipsoid fit of mitochondria to measure mitochondrial elongation.

To analyze the colocalization between ER and mitochondria, TMRM and ERAT4.03 NA were determined on a single cell level using ImageJ and plugin coloc2. The Pearson's coefficient and the Costes thresholded

Manders coefficient were calculated as previously described [44].

2.5. Mitochondrial oxygen consumption rate

As described previously [45], one day before the experiment, respectively treated HeLa cells were plated on XF96 polystyrene cell culture microplates (Seahorse®, Agilent, Vienna, Austria) at a density of 40.000 cells per well. After keeping freshly seeded cells in the incubator at 37 °C for 24 h, the cell culture medium was exchanged with Seahorse medium supplemented with 1 mM sodium pyruvate, 2 mM glutamine, and 5.5 mM D-glucose. The oxygen consumption rate (OCR) was subsequently measured every 7 min using an XF96 extracellular flux analyzer. After basal measurement, 2 μM oligomycin (Sigma Aldrich, Vienna, Austria), 0.4 μM FCCP, and 2.5 μM antimycin were injected. OCR was normalized to protein content using the Pierce™ BCA Protein Assay Kit (Fisher Scientific, Vienna, Austria) assay and presented as $pmolO_2/(min*\mu g_{protein})$ [46].

2.6. Analyses of mRNA expression levels

As described previously [45], the PEQLAB total RNA isolation kit (Erlangen, Germany) was used to isolate the total RNA. The concentration was measured and the purity was controlled with a spectrophotometer (UviLine 9400, SCHOTT Instruments, Mainz, Germany). cDNA transcription was performed using the Applied Biosystems cDNA reverse transcription kit (Foster City, CA). qRT-PCR was done using the QuantiFast SYBR Green RT-PCR kit (Qiagen, Hilden, Germany) and performed on the LightCycler 480 (Roche Diagnostics, Vienna, Austria). Human glyceraldehyde 3-phosphate dehydrogenase (GAPDH) (QuantiTect, Qiagen) was used as a housekeeping gene. The primers used were obtained from Invitrogen (Vienna, Austria) and were as follows:

UCP2: forward: 5'-TCCTGAAAGCCAACCTCATG-3', reverse: 5'-GGCAGAGTTCATGTATCTCGTC-3'; UCP3: forward: 5'-AGAAAATACAGCGGGACTATGG-3', reverse: 5'-CTTGAGGATGTCGTAGGTCAC-3'; PRMT1: forward: 5'-TGCTCAACACCGTGCTCTATGC-3', reverse: 5'-TCCTCGATGGCCGTCACATACA-3'; MCU: forward: 5'AGAGATAGGCTTGAGTGTGAAC-3', reverse: 5'-TTCCTGGCAGAATTTGGGAG-3'; MCUb forward: 5'-TATAGTACCGTGGTGCCACCTGATG-3', reverse: 5'-TTGTAGGTCCTGAAGGAATGAACCA-3', MICU1: forward: 5'-CAGGTTCAGAGCATCATTCG-3', reverse: 5'-GAACACAAGCCAGACTTGAG-3'; LETM1: forward: 5'-TGTTGCTGTGAAGCTCTTCC-3', reverse: 5'-TGTTCTTCAAGGCCATCTCC-3'

2.7. Determination of free T3 concentrations in the cell culture medium

Samples of the respectively treated cell culture medium were collected after indicated incubation times. Samples were stored frozen and protected from light. Then, the levels of free T3 (fT3) were determined by performing an automated chemiluminescence analysis on Advia Centaur (Siemens, Eschborn, Germany) as described previously [47].

2.8. Statistical analyses

The data were analyzed using Microsoft Excel Professional Plus 2019 (Microsoft Corporation, Albuquerque, NM, USA). Statistical analyzes and design of graphs were carried out with GraphPad Prism Version 9.3.0 for Windows (GraphPad Software, San Diego, CA, USA) using Student's *t*-test or one-way ANOVA, if applicable. Data are expressed as MEAN ± SEM unless otherwise indicated. Results were obtained from at least three independent experimental days. Differences were considered statistically significant at $p < 0.05$ and presented as specific p-values (* = $p \leq 0.05$; ** = $p \leq 0.01$; *** = $p \leq 0.001$).

3. Results

3.1. T3 induces an elevation in basal and stimulated $[Ca^{2+}]_{mito}$ levels

Previous work revealed that thyroid hormones boost mitochondrial metabolic activity, enhance the turnover of the TCA cycle, and trigger the ETC and OXPHOS machinery [22,48,49]. The activity of the TCA cycle strongly depends on Ca^{2+}-dependent dehydrogenases in the mitochondrial matrix [33–35]. Consequently, we investigated whether the biologically active thyroid hormone, T3 [1], affects $[Ca^{2+}]_{mito}$. HeLa cells were transfected with the FRET-based $[Ca^{2+}]_{mito}$ sensor 4mtD3cpv and treated with 100 nM T3 for 3 h, 24 h, and 48 h. Live-cell imaging revealed increased basal $[Ca^{2+}]_{mito}$ levels after 3 h but not after 24 h and 48 h of T3 treatment (Fig. 1A and C). Also, $[Ca^{2+}]_{mito}$ uptake after stimulation with 100 μM ATP, inducing IP3-mediated endoplasmic reticulum (ER) Ca^{2+} release, was significantly enhanced after 3 h but not after 24 h and 48 h of T3 treatment (Fig. 1B and C). Since $[Ca^{2+}]_{mito}$ is fueled by cytosolic Ca^{2+} ($[Ca^{2+}]_{cyto}$) [50], we investigated whether T3 affects $[Ca^{2+}]_{cyto}$ homeostasis. Neither basal $[Ca^{2+}]_{cyto}$ (Fig. 1D and F) nor $[Ca^{2+}]_{cyto}$ elevation upon ER Ca^{2+} release by 100 μM ATP (Fig. 1E and F) was altered after T3 incubation for 3 h, 24 h, and 48 h.

3.2. T3 causes upregulation of UCP2, UCP3, and PRMT1

Depending on the source of Ca^{2+}, different Ca^{2+} uptake routes into mitochondria exist [28]. Mitochondrial Ca^{2+} uptake in response to Ca^{2+} depletion of the ER, as shown in Fig. 1B, was found to be dependent on MCU and facilitated by UCP2 [42]. Notably, previous studies reported T3-induced upregulation of UCP2 and UCP3 in adipose tissue cell lines and skeletal muscle [20,51]. Indeed, mRNA expression levels of UCP2 (Fig. 2A) and UCP3 (Fig. 2B), the less abundant isoform of UCPs in HeLa cells, were significantly increased after 3 h of T3 treatment. The expression of UCP2 and UCP3 was decreased after 24 h and normalized in comparison to respective control cells after 48 h. Since the function of UCP2 is dependent on PRMT1-driven methylation of MICU1 [27], we also analyzed mRNA expression levels of PRMT1. Similar to UCP2 and UCP3, PRMT1 mRNA expression levels were enhanced after 3 h, reduced after 24 h, and normalized after 48 h (Fig. 2C). Notably, mRNA expression levels of other proteins involved in $[Ca^{2+}]_{mito}$ uptake upon $[Ca^{2+}]_{ER}$ depletion, including MCU, MCUb, and MICU1, and the mRNA expression of LETM1 (Fig. 2D), a protein contributing to alternative uptake routes [29], were not significantly altered by T3 treatment. Due to the well-known isoform UCP1, UCP2 and UCP3 were assumed to function as uncoupling proteins [52,53]. However, several reports failed to support this assumption, proving that UCP2 and UCP3 do not significantly alter mitochondrial membrane potential [18]. To assess the impact of T3 on mitochondrial membrane potential, we stained respectively treated HeLa cells with TMRM and measured basal mitochondrial membrane potential. Basal mitochondrial membrane potential (Fig. 2E) was normalized to entirely disrupted mitochondrial membrane potential after the application of FCCP [10 μM], which causes the complete release of the TMRM dye into the cytosol (Fig. 2F). T3 treatment for 3 h, 24 h, and 48 h did not alter mitochondrial membrane potential, emphasizing that UCP2 and UCP3 expression does not affect mitochondrial membrane potential. Next, we investigated by 3D-confocal microscopy the structure of mitochondria after T3 treatment through application of the dye TMRM. We found increased mitochondrial volume and surface after 3 h of T3 incubation (Fig. 2G), while the ratio between volume and surface (Fig. 2H), as well as the mitochondrial elongation (Fig. 2I), remained unchanged after T3 treatment in HeLa cells (Fig. 2J). These results indicate a slight increase in mitochondrial size and swelling, potentially due to enhanced basal $[Ca^{2+}]_{mito}$ uptake after T3 application.

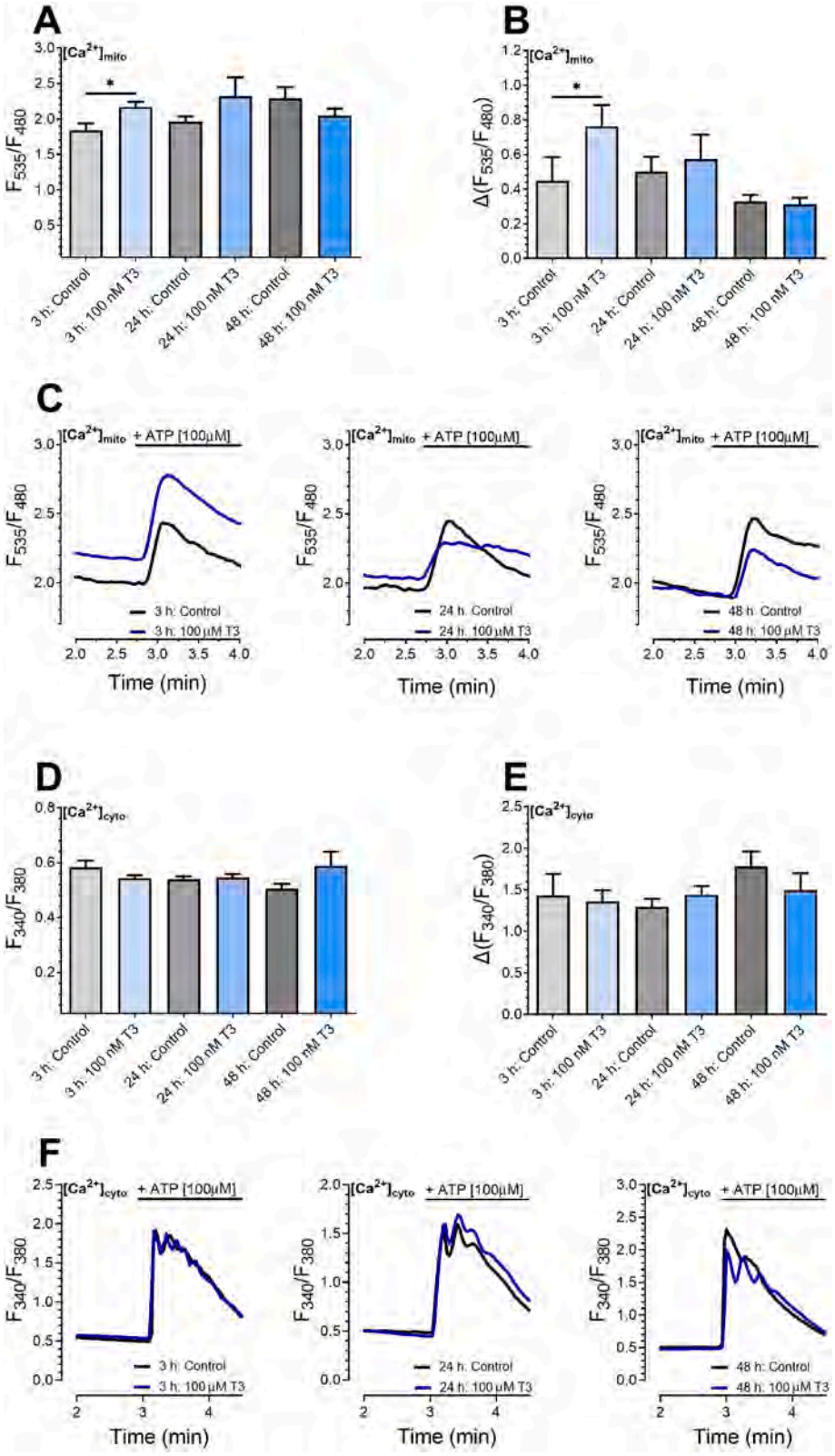

Fig. 1. Effects of T3 on $[Ca^{2+}]_{mito}$ and $[Ca^{2+}]_{cyto}$ homeostasis.

Bar graphs (MEAN + SEM) represent basal $[Ca^{2+}]_{mito}$ levels of control HeLa cells 3 h (n = 42/8/4), 24 h (n = 51/9/4), and 48 h (n = 113/22/6) or HeLa cells treated with 100 nM T3 for 3 h (n = 67/12/4), 24 h (n = 67/11/4), and 48 h (n = 82/14/5) **(1A)**. Bar graphs (MEAN + SEM) represent $[Ca^{2+}]_{mito}$ uptake in response to 100 μM ATP in HeLa cells and in HeLa cells treated with 100 nM T3 for 3 h, 24 h, or 48 h (numbers as for 1A) **(1B)**. Representative $[Ca^{2+}]_{mito}$ traces of control HeLa cells (black curves) or HeLa cells treated with 100 nM T3 (blue curves) for 3 h *(left)*, 24 h *(middle)*, or 48 h *(right)* **(1C)**. Bar graphs (MEAN + SEM) represent basal $[Ca^{2+}]_{cyto}$ levels of control HeLa cells treated for 3 h (n = 73/9/3), 24 h (n = 83/11/3), and 48 h (n = 82/12/3) or HeLa cells treated with 100 nM T3 for 3 h (n = 65/11/3), 24 h (n = 93/12/3), or 48 h (n = 76/12/3) **(1D)**. Bar graphs (MEAN + SEM) represent $[Ca^{2+}]_{cyto}$ elevation in response to 100 nM ATP in control HeLa cells or HeLa cells treated with 100 nM T3 for 3 h, 24 h, or 48 h **(1E)**. Representative $[Ca^{2+}]_{cyto}$ traces of control HeLa cells (black curves) or HeLa cells treated with 100 nM T3 (blue curves) for 3 h *(left)*, 24 h *(middle)*, and 48 h *(right)* **(1F)**. Results were obtained in at least 3 independent experiments (n ≥ 3). If applicable, significant differences were assessed via one-way ANOVA or unpaired *t*-test and presented as specific p-values (* = $p \leq 0.05$, ** = $p \leq 0.01$, *** = $p \leq 0.001$). (For interpretation of the references to colour in this figure legend, the reader is referred to the Web version of this article.)

3.3. T3's impact on $[Ca^{2+}]_{mito}$ is dependent on UCP2-dependent Ca^{2+} uptake

To directly test whether the function of proteins involved in $[Ca^{2+}]_{mito}$ uptake is essential to T3's effect on $[Ca^{2+}]_{mito}$ homeostasis, we performed experiments in 4mtD3cpv expressing HeLa cells depleted from proteins of interest. As already shown in Fig. 1A and B, basal $[Ca^{2+}]_{mito}$ levels (Fig. 3A) and $[Ca^{2+}]_{mito}$ uptake (Fig. 3B) were significantly increased after 3 h of treatment with 100 nM T3. A UCP2-dependent $[Ca^{2+}]_{mito}$ uptake requires functional MCU [42] as well as PRMT1-driven methylation [27]. Indeed, the application of siRNA against MCU abolished the effect of T3 on basal $[Ca^{2+}]_{mito}$ levels

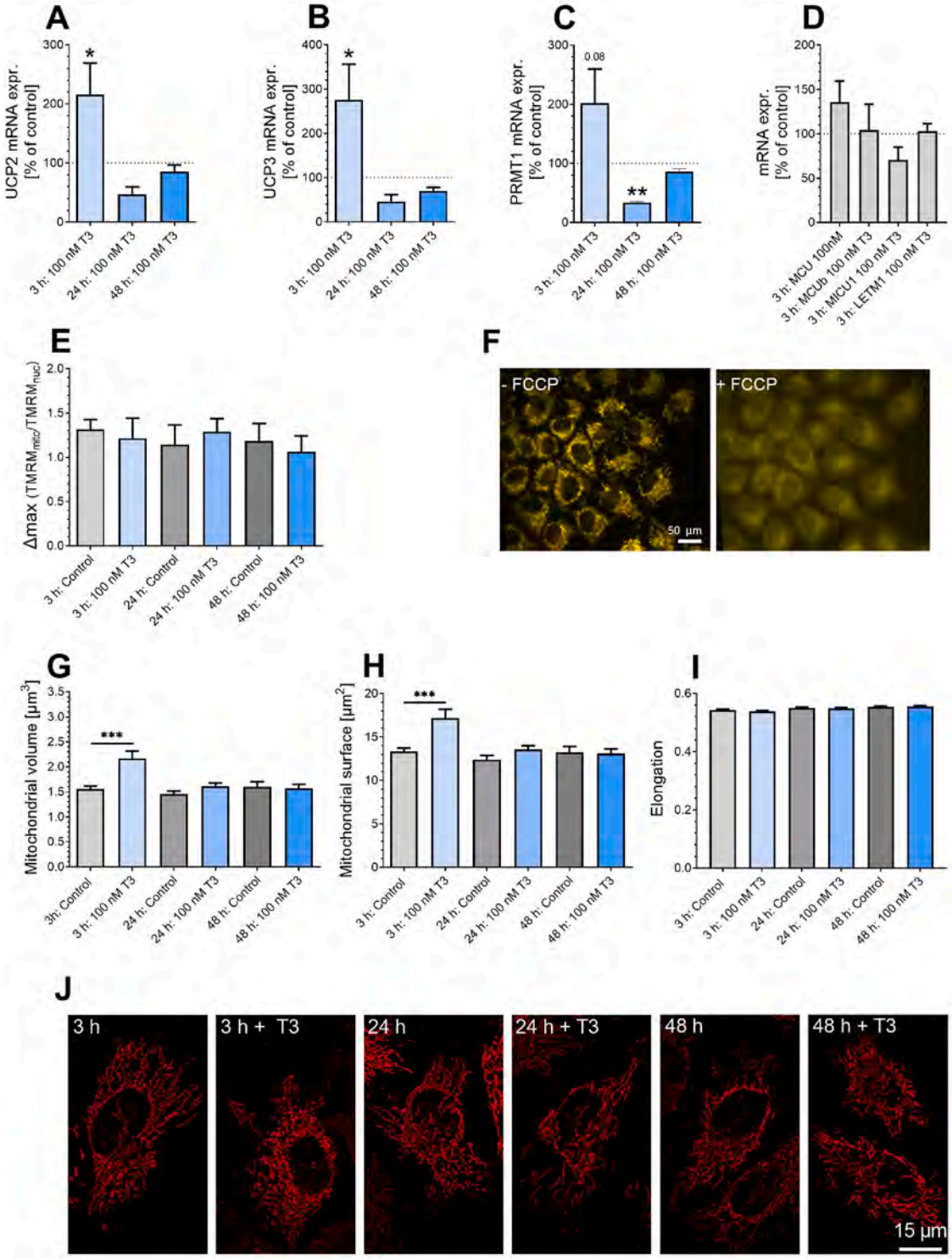

Fig. 2. T3's impact on mRNA expression, mitochondrial membrane potential, and mitochondrial structure.
Bar graphs (MEAN ± SEM) represent the percentage of UCP2 mRNA expression level change in HeLa treated with 100 nM T3 for 3 h (n = 6), 24 h (n = 3), or 48 h (n = 3) compared to respective control cells **(2A).** Bar graphs (MEAN ± SEM) represent the percentage of UCP3 mRNA expression level change in HeLa cells treated with 100 nM T3 for 3 h (n = 5), 24 h (n = 3), or 48 h (n = 3) compared to respective control cells **(2B).** Bar graphs (MEAN ± SEM) represent the percentage of PRMT1 mRNA expression level change of HeLa cells treated with 100 nM T3 for 3 h (n = 7), 24 h (n = 3), or 48 h (n = 3) compared to respective control cells **(2C)**. Bar graphs (MEAN ± SEM) represent the percentage of MCU, MCUb, MICU1 and LETM1 mRNA expression of HeLa cells treated with 100 nM T3 for 3 h (n = 5) compared to respective control cells **(2C).** Bar graphs (MEAN ± SEM) reveal mitochondrial membrane potential normalized to fully disrupted mitochondrial membrane potential in response to FCCP [10 µM] in control HeLa cells for 3 h (n = 30/7/3), 24 h (n = 30/7/3) or 48 h (n = 31/8/3) and in HeLa cells treated with 100 nM T3 for 3 h (n = 30/7/3), 24 h (n = 30/7/3), or 48 h (n = 37/9/3) **(2E)**. Cells stained with TMRM before *(left)* and after *(right)* application of FCCP **(2F)**. Bar graphs (MEAN ± SEM) represent mitochondrial volume **(2G)**, surface, **(2H)** and elongation **(2I)** of control HeLa (n = 71/8/4), 24 h (n = 80/8/4), or 48 h (n = 72/8/4) or HeLa cells treated with 100 nM T3 for 3 h (n = 75/8/4), 24 h (n = 80/8/4), or 48 h (n = 71/8/4). Representative images show TMRM-stained control HeLa cells and HeLa cells treated with T3 for 3 h *(left)*, 24 h *(middle)*, and 48 h *(right)* **(2J)**. Results were obtained in at least 3 independent experiments (n ≥ 3). If applicable, significant differences were assessed via one-way ANOVA or unpaired *t*-test and presented as specific p-values (* = p ≤ 0.05, ** = p ≤ 0.01, *** = p ≤ 0.001).

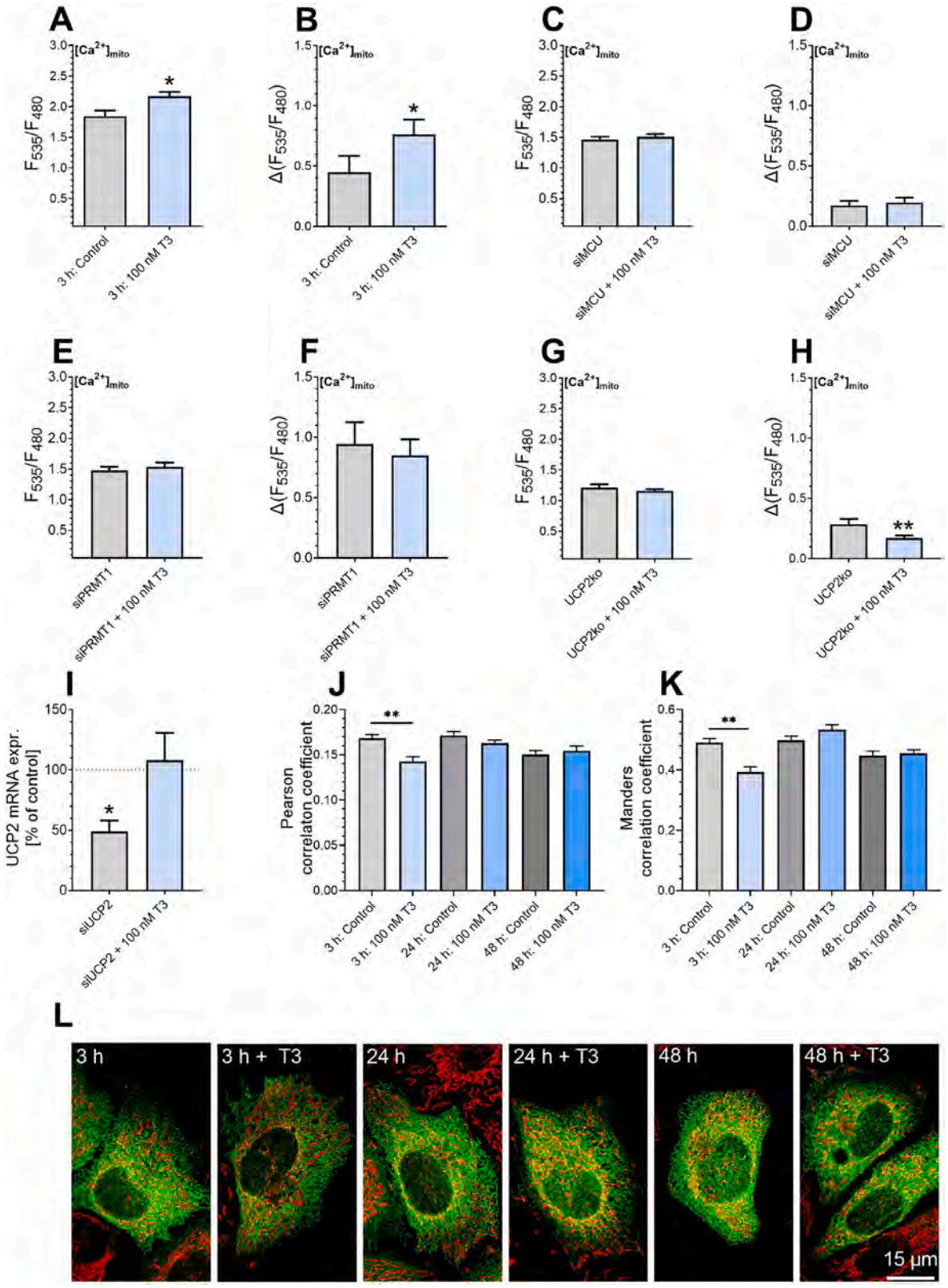

(caption on next page)

Fig. 3. Effects of T3 on $[Ca^{2+}]_{mito}$ homeostasis of HeLa cells with transient knockdown of MCU and PRMT1 and HeLa cells with a stable knockout of UCP2. Bar graphs (MEAN + SEM) represent basal $[Ca^{2+}]_{mito}$ levels of control HeLa cells (n = 42/8/4) or HeLa cells treated with 100 nM T3 for 3 h (n = 67/12/4), shown in Fig. 1A (3A). Bar graphs (MEAN + SEM) represent $[Ca^{2+}]_{mito}$ uptake in response to 100 μM ATP in control HeLa cells (n = 42/8/4) or HeLa cells treated with 100 nM T3 for 3 h (n = 67/12/4), shown in Fig. 1B (3B). Bar graphs (MEAN + SEM) represent basal $[Ca^{2+}]_{mito}$ levels of control HeLa cells transfected with siRNA against MCU (n = 40/19/4) or respective HeLa cells treated with 100 nM T3 for 3 h (n = 49/20/4) (3C). Bar graphs (MEAN + SEM) represent $[Ca^{2+}]_{mito}$ uptake in response to 100 μM ATP in control HeLa cells transfected with siRNA against MCU (n = 40/19/4) or respective HeLa cells treated with 100 nM T3 for 3 h (n = 49/20/4) (3D). Bar graphs (MEAN + SEM) represent basal $[Ca^{2+}]_{mito}$ levels of HeLa cells transfected with siRNA against PRMT1 (n = 55/27/5) or of respective HeLa cells treated with 100 nM T3 for 3 h (n = 49/25/5) (3E). Bar graphs (MEAN + SEM) represent $[Ca^{2+}]_{mito}$ uptake in response to 100 μM ATP in HeLa cells transfected with siRNA against PRMT1 (n = 55/27/5) or in respective HeLa cells treated with 100 nM T3 for 3 h (n = 49/25/5) (3F). Bar graphs (MEAN + SEM) represent basal $[Ca^{2+}]_{mito}$ levels of control HeLa cells with stable knockout of UCP2 (n = 29/9/3) or respective cells treated with 100 nM T3 for 3 h (n = 33/9/3) (3G). Bar graphs (MEAN + SEM) represent $[Ca^{2+}]_{mito}$ uptake in response to 100 μM ATP in HeLa cells with stable knockout of UCP2 (n = 29/9/3) or respective HeLa cells treated with 100 nM T3 for 3 h (n = 33/9/3) (3H). Bar graphs (MEAN ± SEM) represent the percentage of UCP2 mRNA expression level change in HeLa cells treated with siRNA against UCP2 and HeLa cells treated with siRNA against UCP2 and 100 nM T3 (n = 4) (3I). Bar graphs (MEAN + SEM) show Pearson's (3J) and Manders's 2 (3K) of control HeLa (n = 71/8/4), 24 h (n = 80/8/4), or 48 h (n = 72/8/4) or HeLa cells treated with 100 nM T3 for 3 h (n = 75/8/4), 24 h (n = 80/8/4), or 48 h (n = 71/8/4). Representative picture show control TMRM stained and ERAT4.0NA expressing control HeLa cells and respective HeLa cells treated with T3 for 3 h, 24 h, and 48 h. Mitochondria are depicted in red, the ER in green, and overlapping areas in yellow (3L). Results were obtained in at least 3 independent experiments (n ≥ 3). If applicable, significant differences were assessed via one-way ANOVA or unpaired *t*-test and presented as specific p-values (* = p ≤ 0.05, ** = p ≤ 0.01, *** = p ≤ 0.001). (For interpretation of the references to colour in this figure legend, the reader is referred to the Web version of this article.)

(Fig. 3C) and on $[Ca^{2+}]_{mito}$ uptake upon IP3-generating agonist response (Fig. 3D). Also, knockdown of PRMT1 prevented the effect of T3 under basal conditions (Fig. 3E) and after intracellular Ca^{2+} release (Fig. 3F). Next, we tested whether T3 application affects $Ca^{2+}]_{mito}$ levels in UCP2 knockout HeLa cells. The basal $[Ca^{2+}]_{mito}$ remained unchanged by T3 application (Fig. 3G), while the $[Ca^{2+}]_{mito}$ uptake was significantly decreased after T3 treatment for 3 h (Fig. 3H), possibly due to hampered MICU1 activity as a result of PRMT1 upregulation (Fig. 2C) and the lack of UCP2 [39]. The usage of UCP2 knockout HeLa has become necessary since incubation with 100 nM T3 counteracts siRNA-induced knockdown of UCP2 (Fig. 3I). A former report has revealed an inverse correlation between UCP2 mRNA expression and ER-mitochondrial interaction [44]. Consequently, we aimed to test whether upregulation of UCP2 induced by T3 is also accompanied by alterations in the colocalization between ER and mitochondria. As presented through Pearson's (Fig. 3J) and Mander's 2 (Fig. 3K) coefficients, the interaction between mitochondria and ER was reduced after 3 h of T3 treatment in TMRM stained and ERAT4.0NA expressing HeLa (Fig. 3L). Notably, at this time point, the mRNA expression level of UCP2 was found to be enhanced (Fig. 2A). In line with the mRNA expression level of UCP2, the ER-mitochondrial interaction was normalized to respective control levels after 48 h.

3.4. T3's impact on mitochondrial ATP and ROS production is dependent on $[Ca^{2+}]_{mito}$

Thyroid hormones are known to boost cellular metabolism [54]. Notably, $[Ca^{2+}]_{mito}$ is essential to the function of Ca^{2+}-dependent matrix dehydrogenases [33–35,55]. To determine after which incubation period T3 affects mitochondrial metabolism, we measured basal oxygen consumption rate (OCR) and the OCR after application of the ATP synthase inhibitor oligomycin, the uncoupling agent FCCP, and the inhibitor of complex III antimycin A. Incubation of HeLa cells with 100 nM T3 for 3 h enhanced basal OCR (Fig. 4A) and boosted maximal OCR after FCCP application significantly (Fig. 4B). No alterations could be observed after 24 h and 48 h of T3 incubation compared to respective controls. To analyze whether enhanced OCR also correlates with enhanced mitochondrial ATP production, we measured mitochondrial ATP ($[ATP]_{mito}$) levels by using the organelle-targeted ATP sensor mtAT1.03 after treatment with T3 for 3 h. Notably, basal $[ATP]_{mito}$ levels were significantly elevated after 3 h of T3 treatment in HeLa cells (Fig. 4D), while transient siRNA-induced knockdown of MCU (Fig. 4E) and of PRMT1 (Fig. 4F) abolished the effect of T3 on $[ATP]_{mito}$ levels. Also, $[ATP]_{mito}$ levels remained unchanged after T3 treatment in UCP2 knockout HeLa (Fig. 4G). Enhanced OCR and $[ATP]_{mito}$ require a boost in the ETC activity, one of the main cellular production sites for reactive oxygen species (ROS) [56]. To investigate whether T3 also affects ROS levels after 3 h of incubation, we expressed the mitochondrial H_2O_2 ($[H_2O_2]_{mito}$) sensor, HyPer [43], in HeLa cells and measured basal $[H_2O_2]_{mito}$ levels. In line with enhanced mitochondrial respiration activity, basal ROS levels were increased after 3 h of T3 treatment (Fig. 4H). These basal levels were normalized to maximal $[H_2O_2]_{mito}$ levels induced by the application of 150 μM H_2O_2 (Fig. 4J). T3 application did not cause a significant rise in $[H_2O_2]_{mito}$ levels in UCP2 knockout HeLa cells (Fig. 4I and J), supporting the concept of an important role of mitochondrial Ca^{2+} uptake in mitochondrial ROS formation in response to T3. Notably, ROS scavenging by treatment with 5 mM NAC for 3 h significantly enhanced basal $[Ca^{2+}]_{mito}$ levels (Fig. 4K) and mitochondrial Ca^{2+} uptake (Fig. 4L). No significant impact of T3 on basal $[Ca^{2+}]_{mito}$ levels (Fig. 4K) and mitochondrial Ca^{2+} uptake (Fig. 4L) could be detected in NAC-treated cells. These results suggest that ROS scavenging by NAC affects $[Ca^{2+}]_{mito}$ homeostasis, potentially covering T3's impact, but might also point to an essential role of ROS as signaling molecules to adjust $[Ca^{2+}]_{mito}$ homeostasis in response to T3.

4. Discussion

Thyroid hormones are key determinants of cellular metabolism, modulating the pathways to metabolize carbohydrates, lipids, and proteins in various tissues [48]. Since a proper mitochondrial Ca^{2+} homeostasis is essential to boost the activity of Ca^{2+}-dependent dehydrogenases like pyruvate dehydrogenase, isocitrate dehydrogenase, and α-ketoglutarate dehydrogenase of the TCA-cycle [33–35], $[Ca^{2+}]_{mito}$ serves as a potent regulator of the mitochondrial metabolism [55]. Consequently, it appears fundamental that T3-induced enhancement of cellular metabolism is accompanied by an adjustment of $[Ca^{2+}]_{mito}$ homeostasis (Fig. 1A and B), enabling enhanced dehydrogenases activity. Studies in mitochondria isolated from the liver of hyperthyroid rats have already suggested enhanced $[Ca^{2+}]_{mito}$ uptake by increased expression of MCU [57]. A recent study suggested a boost in the intracellular Ca^{2+} and revealed that T3 treatment hampers protein degradation mediated by mechanistic target of rapamycin (mTOR), causing increased protein abundance of UCP1 and MCU in brown adipocytes of mice within 30 min [58]. Also, T3 was found to rapidly and transiently increase $[Ca^{2+}]_{cyto}$ levels within several minutes in rat myocytes [59]. The rapid alterations on cellular Ca^{2+} levels found in brown adipocytes of mice and rat myocytes suggest that T3 might modulate cellular Ca^{2+} initially in a non-canonical way. Notably, we could neither detect rapid changes in cytosolic Ca^{2+} levels within short-term T3 incubation nor after 3 h, 24 h, or 48 h (Fig. 1D and E) in HeLa cells. Consequently, we assume that T3-induced rapid changes in cellular Ca^{2+} homeostasis are tissue-specific and that effects on $[Ca^{2+}]_{mito}$ levels of HeLa cells after 3 h of T3 incubation are conveyed through the canonical pathway by specific modulation of gene

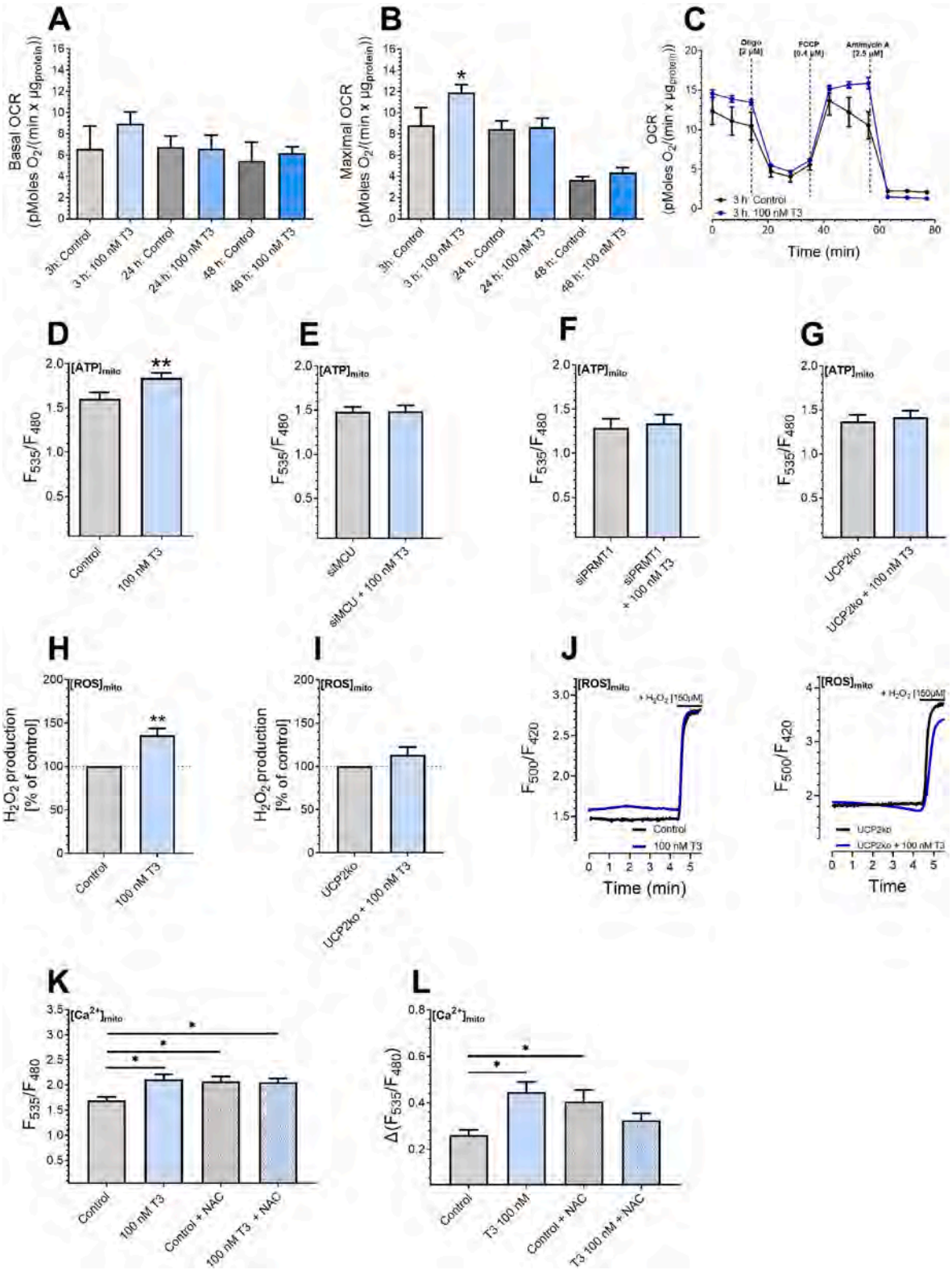

(caption on next page)

Fig. 4. Effects of T3 on mitochondrial metabolism and ROS production in HeLa cells.
Basal OCR presented as MEAN ± SEM before injection of compounds in control HeLa cells and HeLa cells treated with 100 nM T3 for 3 h (n = 3), 24 h (n = 3), or 48 h (n = 3) **(4A)**. Maximal OCR (MEAN ± SEM) in response to FCCP in control HeLa cells and in HeLa cells treated with 100 nM T3 for 3 h (n = 3), 24 h (n = 3), or 48 h (n = 3) **(4B)**. Representative OCR changes in control HeLa cells (black curve) or HeLa cells treated with 100 nM T3 for 3 h (blue curve) **(4C).** Bar graphs (MEAN ± SEM) represent basal $[ATP]_{mito}$ levels of control HeLa cells for 3 h (n = 24/10/3) or treated with 100 nM T3 for 3 h (n = 18/8/3) **(4D)**. Bar graphs (MEAN ± SEM) represent basal $[ATP]_{mito}$ levels in control HeLa cells transfected with siRNA against MCU (n = 49/25/3) or respective HeLa cells treated with 100 nM T3 for 3 h (n = 40/20/3) **(4E).** Bar graphs (MEAN ± SEM) represent basal $[ATP]_{mito}$ levels in control HeLa cells transfected with siRNA against PRMT1 (n = 40/19/4) or respective HeLa cells treated with 100 nM T3 for 3 h (n = 38/19/4) **(4F).** Bar graphs (MEAN ± SEM) represent basal $[ATP]_{mito}$ levels in control HeLa cells with stable UCP2 knockout (n = 109/31/6) and in respective HeLa cells treated with 100 nM T3 for 3 h (n = 110/34/6) **(4G).** Bar graphs (MEAN ± SEM) represent $[H_2O_2]_{mito}$ production of HeLa cells treated with 100 nM T3 for 3 h (n = 41/9/4) compared to respective control cells (n = 44/10/4) **(4H).** Bar graphs (MEAN ± SEM) represent $[H_2O_2]_{mito}$ production of HeLa cells with UCP2 knockout treated with 100 nM T3 for 3 h (n = 47/12/4) compared to respective control cells (n = 41/14/4) **(4I).** Representative $[H_2O_2]_{mito}$ traces of control *(left)* and UCP2 knockout *(right)* HeLa cells (black curves) or respective HeLa cells treated with 100 nM T3 for 3 h (blue curves), before and after addition of 150 μM H_2O_2 **(4J)**. Bar graphs (MEAN + SEM) represent basal $[Ca^{2+}]_{mito}$ levels of control HeLa cells (n = 101/26/6), treated with 100 nM T3 (n = 105/26/6), 5 mM NAC (n = 108/26/6), or both (n = 116/26/6) **(4K)**. Bar graphs (MEAN + SEM) represent $[Ca^{2+}]_{mito}$ uptake in response to 100 μM ATP in control HeLa cells cells (n = 101/26/6), treated with 100 nM T3 (n = 105/26/6), 5 mM NAC (n = 108/26/6), or both (n = 116/26/6) **(4L)**.
Results were obtained in at least 3 independent experiments (n ≥ 3). If applicable, significant differences were assessed via one-way or two-way ANOVA, or unpaired *t*-test and presented as specific p-values (* = p ≤ 0.05, ** = p ≤ 0.01, *** = p ≤ 0.001). (For interpretation of the references to colour in this figure legend, the reader is referred to the Web version of this article.)

expression levels.

Just a limited number of genes are actually controlled in their expression by thyroid hormones, including UCP2 and UCP3 [20–22]. In HeLa cells that exhibit TRα and TRβ [60], incubation with 100 nM T3 in an FCS-containing medium caused a significant upregulation of UCP2 (Fig. 2A), the less abundant UCP3 (Fig. 2B), and PRMT1 (Fig. 2C) after 3 h. Others reported an increase of UCP2 and UCP3 after treatment with 100 nM of T3 in human muscle cells after 24 h incubation [20]. Also, *in vivo* experiments have revealed upregulation of UCP2 and UCP3 in mice [21], rats [22], and humans after different treatment periods [20]. In contrast, reduced UCP2 mRNA expression levels were found in patients with hypothyroidism [23]. Since the impact of the biologically active T3 [61] is determined by deiodinase activities, transport mechanisms [62], and the density of the respective receptors [63], we assume that the timing of T3's impact on gene expression is tissue- and cell-specific. Notably, UCP2 has a half-life of 30 min [64] and UCP3 of 30 min to 4 h [65]. This high protein turnover of UCP2 and UCP3 is in strong contrast to UCP1 with a half-life of 30 h [64,65] and fits to an expression level change induced by T3 within 3 h (Fig. 2A and B). PRMT1, which is essential for UCP2's function in modulating $[Ca^{2+}]_{mito}$, was also found to be upregulated after 3 h of T3 treatment (Fig. 2C). Previous experiments in the frog *Xenopus laevis* reported T3-induced upregulation of PRMT1 expression [66] and revealed that PRMT1 acts as a T3 receptor coactivator [67], hinting at a boosting effect of PRMT1 on T3 activity.

The mRNA expression levels from UCP2 (Fig. 2A), UCP3 (Fig. 2B), and PRMT1 (Fig. 2C) were reduced after 24 h and normalized after 48 h. Notably, treatment with 100 nM T3 caused a significant rise in the level of free fT3 in the cell culture medium (Supplementary Fig. 1). After 3 h of T3 incubation, levels of fT3 dropped significantly. Then, fT3 levels remained stable for 24 h and 48 h. These results might indicate that T3 gets bound initially and remains stable without further degradation or binding within 48 h. Consequently, we assume that alterations in $[Ca^{2+}]_{mito}$ induce adaptational responses in respectively treated cells after 24 h. Still, we can't exclude that T3 gets inactivated by intracellular degradation [48]. In line with that, oral administration of T3 causes peak levels in the blood after 2–4 h, making frequent dosing of T3 necessary and the treatment with the more stable thyroxine, T4, more attractive [61,68]. The reported upregulation of UCP2 and UCP3 in mice [21], rats [22], and humans [20] after daily thyroid hormone administration suggests that the effect seen after 3 h might be maintained over a prolonged period by frequent dosing.

T3-induced upregulation of UCP2 and UCP3 was not accompanied by alterations in mitochondrial membrane potential (Fig. 2 E), opposing a potential function of UCP2 and UCP3 as uncouplers. Early reports showed that UCP2 and UCP3 affect mitochondrial membrane potential in yeast [52,53]. However, these effects were declared artifacts due to an extraordinarily high level of overexpression in experimental models [69]. In fact, UCP2 and UCP3 merely account for 0.01% to 0.1% of IMM proteins in mammalian cells [16]. This fits to *in vivo* studies reporting a direct correlation between mRNA expression levels of UCP2 and UCP3 and the rate of resting metabolic rate in mice [21] and enhanced UCP2 and UCP3 expression accompanied by ATP production in rats [22]. Also, experiments in different cell types failed to reveal alterations in mitochondrial membrane potential induced by UCP2 and UCP3 [17,18].

To elucidate the role of different proteins in the effect of T3 on mitochondrial Ca^{2+}, we tested T3's effect on cells depleted of MCU, PRMT1, and UCP2. Our experiments revealed that the impact of T3 on mitochondrial Ca^{2+} homeostasis is dependent on MCU (Fig. 3C and D), PRMT1 (3E, 3F), and UCP2 (Fig. 3G and H). Due to the low abundance of UCP3 in HeLa cells [70], we solely tested for UCP2 function. Notably, T3 incubation normalized UCP2 expression levels in HeLa cells treated with siRNA against UCP2 (Fig. 3I). Consequently, we performed experiments in HeLa with Crispr/Cas9-induced knockout of UCP2 [39]. In 2007, UCP2 and UCP3 were characterized as fundamental proteins for $[Ca^{2+}]_{mito}$ uptake [18]. Further studies revealed the intermembrane loop 2 (IML2) as an essential protein part of UCP2 and UCP3 for mitochondrial Ca^{2+} modulation [18,28]. They showed that UCP2 and UCP3 normalize mitochondrial Ca^{2+} uptake in the case of PRMT1-driven desensitization of MICU1's Ca^{2+} binding [27] in cancer cells [45]. Thereby, UCP2 and UCP3 modulate the mitochondrial Ca^{2+} uptake via the MCU in response to IP3-generating agonist stimulation [71]. We assume that T3 induces alterations on mitochondrial Ca^{2+} homeostasis via an MCU-dependent uptake route modulated by UCP2 and PRMT1. As shown in Fig. 3H, T3 treatment caused a significant decrease in the mitochondrial Ca^{2+} uptake of UCP2 knockout HeLa. We hypothesize that T3-induced PRMT1 upregulation prevented proper mitochondrial Ca^{2+} uptake in these HeLa cells lacking the normalizing function of UCP2. Further, a reduction of ER-mitochondrial contact sides, which serve as the main hubs for Ca^{2+} signaling between these organelles, after T3 incubation might cause a decrease in mitochondrial Ca^{2+} uptake. In addition to the impact of T3 on mitochondrial Ca^{2+} homeostasis, T3 might also affect the transport of fatty acid transport [24,25] or TCA cycle intermediates [26] by modulating UCP2 expression. How these effects add to the T3-induced modulation of mitochondrial metabolic activity has to be further elaborated.

Notably, previous reports revealed that an inverse correlation between UCP2 expression and the stability of mitochondrial-ER interaction serves as a mechanism for cancer cells to protect themselves from mitochondrial Ca^{2+} overload [45]. This fits our results obtained by confocal microscopy showing decreased interaction between ER and mitochondria after 3 h of T3 treatment (Fig. 3J and K) when UCP2 and UCP3 mRNA expression levels were found to be elevated (Fig. 2A and B). Therefore, we assume that also T3-induced upregulation of UCP2 and UCP3 provokes adaptation of the ER-mitochondrial interplay to prevent

Ca^{2+} overload-induced apoptosis.

We revealed that OCR (Fig. 4A and B), as well as mitochondrial ATP levels (Fig. 4D), rise significantly after 3 h of T3 incubation. These results, again, oppose the hypothesis that UCP2 and UCP3 function as uncouplers and are aligned with results obtained from *in vivo* experiments in rats, presenting an increase in UCP2 and UCP3 expression and mitochondrial ATP production after T3 treatment [22]. Notably, knockdown of MCU (Fig. 4E) and PRMT1 (Fig. 4F) as well as knockout of UCP2 (Fig. 4F) prevented the impact of T3 on mitochondrial ATP levels, emphasizing the crucial role of mitochondrial Ca^{2+} homeostasis on OXPHOS activity. The ETC is the primary cellular ROS production site, and enhanced activity might yield ROS [72]. As presented in Fig. 4H, the basal $[H_2O_2]_{mito}$ was indeed enhanced after 3 h of T3 treatment. Previous reports have shown that severe hyperthyroidism is associated with increased ROS production, promoting mitochondrial biogenesis and mitophagy and, thus, mitochondrial turnover and cellular health [10]. As shown in Fig. 4I, the impact of T3 on basal $[H_2O_2]_{mito}$ levels was abolished in UCP2 knockout HeLa. Consequently, we assume that mitochondrial ROS formation in response to T3 is at least partly dependent on enhanced mitochondrial Ca^{2+} uptake. ROS formation induced by increased mitochondrial Ca^{2+} uptake might, in turn, modulate proteins involved in mitochondrial Ca^{2+} homeostasis. Notably, so far, no impact of UCP2 on basal $[Ca^{2+}]_{mito}$ levels could be revealed, but an elevation of basal mitochondrial Ca^{2+} was observed in our experiments after T3 treatment (Fig. 3A). We assume that post-translational modifications by ROS might cause elevated basal $[Ca^{2+}]_{mito}$ after T3 incubation. ROS were, for instance, shown to modulate the activity of IP3 receptor [73,74] and SERCA [75] isoforms. Moreover, MCU is controlled by ROS via S-glutathionylation at cysteine 97, boosting the MCU channel assembly into higher-order complexes with persistent activity [38]. Based on these studies, ROS-induced alterations in the ER to mitochondrial Ca^{2+} flux as well as in the mechanism of mitochondrial Ca^{2+} uptake might affect basal $[Ca^{2+}]_{mito}$.

Notably, ROS scavenging by NAC application caused an elevation in basal $[Ca^{2+}]_{mito}$ levels (Fig. 4K) and agonist-triggered mitochondrial Ca^{2+} uptake (Fig. 4L). We assume that the antioxidant and the reducing activity of NAC might affect $[Ca^{2+}]_{mito}$ signaling by altering protein function via, for instance, disruption of disulfide bonds [76]. In this regard, it is interesting that the absence of the disulfide bond between MICU1 and MICU2 has been shown to boost mitochondrial Ca^{2+} uptake due to the lack of MICU2's inhibiting function on MICU1 [77]. In NAC-treated cells, no further impact of T3 on basal $[Ca^{2+}]_{mito}$ levels (Fig. 4K) was detected. However, T3 induced a reduction in agonist-triggered mitochondrial Ca^{2+} uptake in NAC-treated cells (Fig. 4L). Notably, MCU's shuttling to the IBM was proven essential to the UCP2- and PRMT1- dependent mitochondrial Ca^{2+} uptake in HeLa cells [39]. Consequently, a reduction in mitochondrial Ca^{2+} uptake might be due to a hampered MCU shuttling to the inner boundary membrane (IBM) by ROS scavenging under a physiological level. Notably, oxidation of MCU was found to facilitate MCU's accumulation in the IBM [38]. Consequently, it is tempting to speculate that ROS scavenging by NAC might prevent MCU shuttling to the IBM and thereby inhibit a T3-facilitated mitochondrial Ca^{2+} uptake in HeLa cells dependent on UCP2 and PRMT1. Moreover, ROS scavenging might impair the activity of UCP2 and UCP3 [78], potentially hampering UCP2's function to reestablish mitochondrial Ca^{2+} uptake under conditions of high PRMT1 levels [27]. However, these are mere speculations, and further experiments are required to clarify how ROS and Ca^{2+} homeostasis are intertwined in T3 signaling.

5. Conclusions

The current study reveals that T3 causes enhanced basal $[Ca^{2+}]_{mito}$ by facilitating an UCP2-dependent and PRMT1-controlled mitochondrial Ca^{2+} uptake via MCU. T3's impact on $[Ca^{2+}]_{mito}$ correlates with the expression and activity of UCP2 and translates into enhanced $[ATP]_{mito}$ and $[H_2O_2]_{mito}$ production. These results suggest that mitochondrial Ca^{2+} homeostasis is essential for the role of T3 in controlling metabolic activity.

Author contributions

I.T., B.G., A.J, D.B., and R.R. performed experiments and analyzed the data. B.O.-P. provided the fT3 analysis. C.M.-S. planned and wrote the manuscript together with B.G. and W.F.G. Funding was acquired by C.M.-S., B.G., and W.F.G. All authors have read and agreed to the published version of the manuscript.

Funding

This work was funded by the Austrian Science Fund (FWF) (J4205-B27 to C.M.-S., DK-MCD W1226 to W.F.G.) and the MEFOgraz (to C.M.-S., W.F.G., and B.G.).

Declaration of competing interest

The authors declare no conflict of interest.

Appendix A. Supplementary data

Supplementary data to this article can be found online at https://doi.org/10.1016/j.freeradbiomed.2022.01.024.

References

[1] M. Plateroti, et al., Thyroid hormones and their receptors: from development to disease, J. Thyroid Res. 2011 (2011) 284737.
[2] G.S. Hones, et al., Noncanonical thyroid hormone signaling mediates cardiometabolic effects in vivo, Proc. Natl. Acad. Sci. U. S. A. 114 (52) (2017) E11323–E11332.
[3] J.M. Weitzel, C. Radtke, H.J. Seitz, Two thyroid hormone-mediated gene expression patterns in vivo identified by cDNA expression arrays in rat, Nucleic Acids Res. 29 (24) (2001) 5148–5155.
[4] P. Romanque, et al., Thyroid hormone administration induces rat liver Nrf2 activation: suppression by N-acetylcysteine pretreatment, Thyroid 21 (6) (2011) 655–662.
[5] A. Wulf, et al., T3-mediated expression of PGC-1alpha via a far upstream located thyroid hormone response element, Mol. Cell. Endocrinol. 287 (1–2) (2008) 90–95.
[6] S. Baldelli, K. Aquilano, M.R. Ciriolo, PGC-1alpha buffers ROS-mediated removal of mitochondria during myogenesis, Cell Death Dis. 5 (2014) e1515.
[7] L. Pessemesse, et al., Depletion of the p43 mitochondrial T3 receptor in mice affects skeletal muscle development and activity, Faseb. J. 26 (2) (2012) 748–756.
[8] A. Lombardi, et al., Regulation of skeletal muscle mitochondrial activity by thyroid hormones: focus on the "old" triiodothyronine and the "emerging" 3,5-diiodothyronine, Front. Physiol. 6 (2015) 237.
[9] M. Kajimoto, et al., Effects of continuous triiodothyronine infusion on the tricarboxylic acid cycle in the normal immature swine heart under extracorporeal membrane oxygenation in vivo, Am. J. Physiol. Heart Circ. Physiol. 306 (8) (2014) H1164–H1170.
[10] R.A. Sinha, et al., Thyroid hormone induction of mitochondrial activity is coupled to mitophagy via ROS-AMPK-ULK1 signaling, Autophagy 11 (8) (2015) 1341–1357.
[11] B.J. Berry, et al., Use the protonmotive force: mitochondrial uncoupling and reactive oxygen species, J. Mol. Biol. 430 (21) (2018) 3873–3891.
[12] D. Ricquier, F. Bouillaud, The uncoupling protein homologues: UCP1, UCP2, UCP3, StUCP and AtUCP, Biochem. J. 345 Pt 2 (2000) 161–179.
[13] R. Rabelo, et al., Delineation of thyroid hormone-responsive sequences within a critical enhancer in the rat uncoupling protein gene, Endocrinology 136 (3) (1995) 1003–1013.
[14] A.C. Bianco, E.A. McAninch, The role of thyroid hormone and brown adipose tissue in energy homoeostasis, Lancet Diabetes Endocrinol. 1 (3) (2013) 250–258.
[15] Z. Koshenov, et al., The contribution of uncoupling protein 2 to mitochondrial Ca^{2+} homeostasis in health and disease - a short revisit, Mitochondrion 55 (2020) 164–173.
[16] M.D. Brand, T.C. Esteves, Physiological functions of the mitochondrial uncoupling proteins UCP2 and UCP3, Cell Metabol. 2 (2) (2005) 85–93.
[17] N. Li, M. Karaca, P. Maechler, Upregulation of UCP2 in beta-cells confers partial protection against both oxidative stress and glucotoxicity, Redox Biol. 13 (2017) 541–549.
[18] M. Trenker, et al., Uncoupling proteins 2 and 3 are fundamental for mitochondrial Ca^{2+} uniport, Nat. Cell Biol. 9 (4) (2007) 445–452.
[19] A. Lanni, et al., Thyroid hormone and uncoupling proteins, FEBS Lett. 543 (1–3) (2003) 5–10.

[20] P. Barbe, et al., Triiodothyronine-mediated up-regulation of UCP2 and UCP3 mRNA expression in human skeletal muscle without coordinated induction of mitochondrial respiratory chain genes, Faseb. J. 15 (1) (2001) 13–15.
[21] M.B. Jekabsons, et al., T(3) stimulates resting metabolism and UCP-2 and UCP-3 mRNA but not nonphosphorylating mitochondrial respiration in mice, Am. J. Physiol. 277 (2) (1999) E380–E389.
[22] K.R. Short, et al., T(3) increases mitochondrial ATP production in oxidative muscle despite increased expression of UCP2 and -3, Am. J. Physiol. Endocrinol. Metab. 280 (5) (2001) E761–E769.
[23] S. Gjedde, et al., Reduced expression of uncoupling protein 2 in adipose tissue in patients with hypothyroidism, J. Clin. Endocrinol. Metab. 95 (7) (2010) 3537–3541.
[24] M.J. Berardi, J.J. Chou, Fatty acid flippase activity of UCP2 is essential for its proton transport in mitochondria, Cell Metabol. 20 (3) (2014) 541–552.
[25] P. Schrauwen, M.K. Hesselink, The role of uncoupling protein 3 in fatty acid metabolism: protection against lipotoxicity? Proc. Nutr. Soc. 63 (2) (2004) 287–292.
[26] A. Vozza, et al., UCP2 transports C4 metabolites out of mitochondria, regulating glucose and glutamine oxidation, Proc. Natl. Acad. Sci. U. S. A. 111 (3) (2014) 960–965.
[27] C.T. Madreiter-Sokolowski, et al., PRMT1-mediated methylation of MICU1 determines the UCP2/3 dependency of mitochondrial Ca^{2+} uptake in immortalized cells, Nat. Commun. 7 (2016) 12897.
[28] M. Waldeck-Weiermair, et al., The contribution of UCP2 and UCP3 to mitochondrial Ca^{2+} uptake is differentially determined by the source of supplied Ca^{2+}, Cell Calcium 47 (5) (2010) 433–440.
[29] M. Waldeck-Weiermair, et al., Leucine zipper EF hand-containing transmembrane protein 1 (Letm1) and uncoupling proteins 2 and 3 (UCP2/3) contribute to two distinct mitochondrial Ca^{2+} uptake pathways, J. Biol. Chem. 286 (32) (2011) 28444–28455.
[30] P.S. Brookes, et al., Calcium, ATP, and ROS: a mitochondrial love-hate triangle, Am. J. Physiol. Cell Physiol. 287 (4) (2004) C817–C833.
[31] D.B. Zorov, M. Juhaszova, S.J. Sollott, Mitochondrial reactive oxygen species (ROS) and ROS-induced ROS release, Physiol. Rev. 94 (3) (2014) 909–950.
[32] R.M. Denton, Regulation of mitochondrial dehydrogenases by calcium ions, Biochim. Biophys. Acta 1787 (11) (2009) 1309–1316.
[33] R.M. Denton, et al., Regulation of mammalian pyruvate dehydrogenase, Mol. Cell. Biochem. 9 (1) (1975) 27–53.
[34] R.M. Denton, D.A. Richards, J.G. Chin, Calcium ions and the regulation of NAD+-linked isocitrate dehydrogenase from the mitochondria of rat heart and other tissues, Biochem. J. 176 (3) (1978) 899–906.
[35] V.B. Lawlis, T.E. Roche, Regulation of bovine kidney alpha-ketoglutarate dehydrogenase complex by calcium ion and adenine nucleotides. Effects on S0.5 for alpha-ketoglutarate, Biochemistry 20 (9) (1981) 2512–2518.
[36] M.A. Aon, S. Cortassa, B. O'Rourke, Redox-optimized ROS balance: a unifying hypothesis, Biochim. Biophys. Acta 1797 (6–7) (2010) 865–877.
[37] E. Cadenas, A. Boveris, Enhancement of hydrogen peroxide formation by protophores and ionophores in antimycin-supplemented mitochondria, Biochem. J. 188 (1) (1980) 31–37.
[38] Z. Dong, et al., Mitochondrial Ca^{2+} uniporter Is a mitochondrial luminal redox Sensor that augments MCU channel activity, Mol. Cell. 65 (6) (2017) 1014–1028 e7.
[39] B. Gottschalk, et al., MICU1 controls cristae junction and spatially anchors mitochondrial Ca^{2+} uniporter complex, Nat. Commun. 10 (1) (2019) 3732.
[40] M.R. Depaoli, et al., Real-time imaging of mitochondrial ATP dynamics reveals the metabolic setting of single cells, Cell Rep. 25 (2) (2018) 501–512 e3.
[41] Z. Koshenov, et al., Sigma-1 receptor promotes mitochondrial Bioenergetics by orchestrating ER Ca^{2+} Leak during early ER stress, Metabolites 11 (7) (2021).
[42] M. Waldeck-Weiermair, et al., Molecularly distinct routes of mitochondrial Ca^{2+} uptake are activated depending on the activity of the sarco/endoplasmic reticulum Ca^{2+} ATPase (SERCA), J. Biol. Chem. 288 (21) (2013) 15367–15379.
[43] M. Oparka, et al., Quantifying ROS levels using CM-H2DCFDA and HyPer, Methods 109 (2016) 3–11.
[44] C.T. Madreiter-Sokolowski, et al., Dynamic Control of mitochondrial Ca^{2+} Levels as a survival Strategy of cancer cells, Front. Cell Dev. Biol. 9 (2021) 614668.
[45] C.T. Madreiter-Sokolowski, et al., UCP2 and PRMT1 are key prognostic markers for lung carcinoma patients, Oncotarget 8 (46) (2017) 80278–80285.
[46] S. Charoensin, et al., Intact mitochondrial Ca^{2+} uniport is essential for agonist-induced activation of endothelial nitric oxide synthase (eNOS), Free Radic. Biol. Med. 102 (2017) 248–259.
[47] S. Stekovic, et al., Alternate day fasting improves physiological and molecular markers of aging in healthy, non-obese humans, Cell Metabol. 30 (3) (2019) 462–476 e6.
[48] A.G. Cicatiello, D. Di Girolamo, M. Dentice, Metabolic effects of the intracellular regulation of thyroid hormone: old players, new concepts, Front. Endocrinol. 9 (2018) 474.
[49] M.J. Goldenthal, R. Ananthakrishnan, J. Marin-Garcia, Nuclear-mitochondrial cross-talk in cardiomyocyte T3 signaling: a time-course analysis, J. Mol. Cell. Cardiol. 39 (2) (2005) 319–326.
[50] T. Finkel, et al., The ins and outs of mitochondrial calcium, Circ. Res. 116 (11) (2015) 1810–1819.
[51] M.L. Reitman, Y. He, D.W. Gong, Thyroid hormone and other regulators of uncoupling proteins, Int. J. Obes. Relat. Metab. Disord. 23 (Suppl 6) (1999) S56–S59.
[52] C. Fleury, et al., Uncoupling protein-2: a novel gene linked to obesity and hyperinsulinemia, Nat. Genet. 15 (3) (1997) 269–272.
[53] C.Y. Zhang, et al., Assessment of uncoupling activity of uncoupling protein 3 using a yeast heterologous expression system, FEBS Lett. 449 (2–3) (1999) 129–134.
[54] R. Mullur, Y.Y. Liu, G.A. Brent, Thyroid hormone regulation of metabolism, Physiol. Rev. 94 (2) (2014) 355–382.
[55] I. Martinez-Reyes, N.S. Chandel, Mitochondrial TCA cycle metabolites control physiology and disease, Nat. Commun. 11 (1) (2020) 102.
[56] R.Z. Zhao, et al., Mitochondrial electron transport chain, ROS generation and uncoupling (Review), Int. J. Mol. Med. 44 (1) (2019) 3–15.
[57] S.G. Robles, et al., Thyroid hormone may induce changes in the concentration of the mitochondrial calcium uniporter, Comp. Biochem. Physiol. B Biochem. Mol. Biol. 135 (1) (2003) 177–182.
[58] M.T. Nguyen, et al., Thyroid hormone induces Ca^{2+}-mediated mitochondrial Activation in Brown adipocytes, Int. J. Mol. Sci. 22 (16) (2021).
[59] R.B. Lomax, et al., Tri-iodothyronine increases intra-cellular calcium levels in single rat myocytes, J. Mol. Endocrinol. 7 (1) (1991) 77–79.
[60] J.Z. Lin, et al., Gene specific actions of thyroid hormone receptor subtypes, PLoS One 8 (1) (2013) e52407.
[61] J. Jonklaas, et al., Single-dose T3 administration: kinetics and effects on biochemical and physiological parameters, Ther. Drug Monit. 37 (1) (2015) 110–118.
[62] S.M. Abdalla, A.C. Bianco, Defending plasma T3 is a biological priority, Clin. Endocrinol. 81 (5) (2014) 633–641.
[63] A. Schroeder, et al., The ability of thyroid hormone receptors to sense t4 as an agonist depends on receptor isoform and on cellular cofactors, Mol. Endocrinol. 28 (5) (2014) 745–757.
[64] S. Rousset, et al., UCP2 is a mitochondrial transporter with an unusual very short half-life, FEBS Lett. 581 (3) (2007) 479–482.
[65] V. Azzu, S.A. Mookerjee, M.D. Brand, Rapid turnover of mitochondrial uncoupling protein 3, Biochem. J. 426 (1) (2010) 13–17.
[66] K. Fujimoto, et al., Thyroid hormone activates protein arginine methyltransferase 1 expression by directly inducing c-Myc transcription during Xenopus intestinal stem cell development, J. Biol. Chem. 287 (13) (2012) 10039–10050.
[67] L. Xue, et al., Protein arginine methyltransferase 1 regulates cell proliferation and differentiation in adult mouse adult intestine, Cell Biosci. 11 (1) (2021) 113.
[68] P.A. Singer, et al., Treatment guidelines for patients with hyperthyroidism and hypothyroidism. Standards of care committee, American thyroid association, JAMA 273 (10) (1995) 808–812.
[69] J.A. Harper, et al., Artifactual uncoupling by uncoupling protein 3 in yeast mitochondria at the concentrations found in mouse and rat skeletal-muscle mitochondria, Biochem. J. 361 (Pt 1) (2002) 49–56.
[70] E.E. Pohl, et al., Important trends in UCP3 investigation, Front. Physiol. 10 (2019) 470.
[71] M. Waldeck-Weiermair, et al., Spatiotemporal correlations between cytosolic and mitochondrial Ca^{2+} signals using a novel red-shifted mitochondrial targeted cameleon, PLoS One 7 (9) (2012) e45917.
[72] C.T. Madreiter-Sokolowski, C. Thomas, M. Ristow, Interrelation between ROS and Ca^{2+} in aging and age-related diseases, Redox Biol. 36 (2020) 101678.
[73] H. Vais, et al., Redox-regulated heterogeneous thresholds for ligand recruitment among InsP3R Ca^{2+}-release channels, Biophys. J. 99 (2) (2010) 407–416.
[74] H. Ivanova, et al., Inositol 1,4,5-trisphosphate receptor-isoform diversity in cell death and survival, Biochim. Biophys. Acta 1843 (10) (2014) 2164–2183.
[75] K.A. Barnes, S.E. Samson, A.K. Grover, Sarco/endoplasmic reticulum Ca^{2+}-pump isoform SERCA3a is more resistant to superoxide damage than SERCA2b, Mol. Cell. Biochem. 203 (1–2) (2000) 17–21.
[76] G. Aldini, et al., N-Acetylcysteine as an antioxidant and disulphide breaking agent: the reasons why, Free Radic. Res. 52 (7) (2018) 751–762.
[77] C. Petrungaro, et al., The Ca^{2+}-dependent Release of the Mia40-induced MICU1-MICU2 Dimer from MCU regulates mitochondrial Ca^{2+} uptake, Cell Metabol. 22 (4) (2015) 721–733.
[78] R.J. Mailloux, M.E. Harper, Uncoupling proteins and the control of mitochondrial reactive oxygen species production, Free Radic. Biol. Med. 51 (6) (2011) 1106–1115.